

Dust properties of nearby disks: M 31 case

Petko L. Nedialkov¹, Antoniya T. Valcheva²,
Valentin D. Ivanov³ & Leonardo Vanzì⁴

¹Astronomy Department, University of Sofia,
5 J. Bourchier blvd., Sofia 1164, Bulgaria
email: japet@phys.uni-sofia.bg

²Institute of Astronomy,
72 Tsarigradsko Chaussee blvd., Sofia 1784, Bulgaria
email: avalcheva@astro.bas.bg

³European Southern Observatory,
3107 Alonso de Cordova Ave., Casilla 19, Santiago 19001, Chile
email: vivanov@eso.org

⁴Department of Astronomy and Astrophysics, Pontificia Universidad
Católica de Chile, Casilla 306, Santiago 22, Chile
email: lvanzì@eso.org

Abstract. Several properties of the M 31 disk, namely: opacity, extinction law and gas-to-dust ratio are studied by means of optical and near-infrared photometry of ten globular clusters and galaxies seen through the disk. The individual extinctions of these objects were estimated with respect to several sets of theoretical spectral energy distributions for globulars and galaxies. Seven targets are consistent with reddened globulars, two - with starburst galaxies and one - with an elliptical. The extinction estimates agree with semi-transparent disk ($\tau_V \lesssim 1$) in the inter-arm regions. The total-to-selective extinction ratio in those regions 2.75 ± 0.1 is lower on average than the typical Galactic value of $R_V = 3.1$. We also obtained a gas-to-dust ratio, similar to that in the the Milky way. It shows no correlation with the distance from the M31 center.

Keywords. galaxies: ISM, photometry, dust, extinction; globular clusters

1. Introduction

The dust in galaxies attenuates the light of background extragalactic sources. Recent studies (Holwerda et al. 2005) of morphologically representative samples of spirals shows that dust opacity of a disk arises from two distinct components: (*i*) optically thicker ($\tau_V = 0.8 \div 8^m$) and radially dependent component, associated with the spiral arms, and (*ii*) relatively more constant optically thinner disk ($\tau_V \sim 1^m$), dominating the inter-arm regions and the outskirts of the disk.

The nearby giant spiral galaxy M 31 is well suited for comprehensive studies of the interplay between the stars and the ISM. The radial distribution of the opacity in M 31 spiral arms, based on individual estimates towards OB stars, shows that the opacity exponentially decreases away from the bulge (Nedilakov & Ivanov 1998). However, a study of 41 globular clusters in M 31 indicates the absence of radial extinction gradient with the galactocentric distance (Savcheva & Tassev 2002).

Measuring the color excesses of objects behind the disks is an alternative method to constrain the disk opacity. It was applied to M 31 by Cuillandre et al. (2001) who used background galaxies. They concluded that the M31 disk is semi-transparent for distances larger than R_{25} .

Here we complement this work, presenting opacity estimates for galactocentric distance

smaller than R_{25} , derived from the comparison of apparent colors of background globulars and ellipticals with models.

2. Observations and data reduction

Our sample includes 21 background galaxy candidates located well within the standard M 31 radius R_{25} . They were selected from a number of heterogeneous sources: visual inspection of DSS and the NOAO archive photographic plates, dropouts from M 31 globular cluster searches (Battistini et al. 1980). Our original intention was to base the study on background ellipticals only but five of our targets were recently identified as globulars, and their $[\text{Fe}/\text{H}]$ and v_r became readily available from Galleti et al. (2006).

We obtained HK imaging in Dec 1996 and Jan 1997 with ARNICA (Lisi et al. 1993) at 1.8m Vatican Advanced Technology Telescope on Mt. Graham. The instrument is equipped with a NICMOS3 (256×256 pixels) detector array, with scale of 0.505 arc-sec/pixel. The data reduction includes the typical steps for infrared imaging: “sky” removal, flat-fielding, alignment and combination of individual images, separately for every filter and field. Ten of the targets (Table 1, Fig. 1) were identified on the $UBVRI$ images from the Local Group Survey (Massey et al. 2006), obtained with the KPNO Mosaic Camera at 4m Mayall telescope.

Table 1. Sub-set of our original target list, with $UBVRIHK$ photometry.

No.	2MASX/2MASS name	Other name	Object Type ¹	v_r [km s ⁻¹]	$[\text{Fe}/\text{H}]$	r_{gc} [arcmin]	$\text{N}(\text{HI}+2\text{H}_2)^2$ [$\times 10^{20}$ at. cm ⁻²]
1.	2MASX J00451437+4157405	Bol 370	1	-347	-1.80	52.2	1.895
2.	2MASX J00444399+4207298	Bol 250D	1	-442	-	84.2	9.028
3.	2MASS J00420658+4118062	Bol 43D	1	-344	-1.35	30.8	12.836
4.	2MASS J00413428+4101059	Bol 25D	1	-479	-	20.8	0.668
5.	2MASS J00413436+4100497	Bol 26D	1	-465	-1.15	20.8	2.170
6.	2MASS J00413660+4100182	Bol 251	2	-	-	20.6	1.350
7.	2MASS J00430737+4127329	Bol 269	2	-	-	19.6	12.384
8.	2MASS J00421236+4119008	Bol 80	2	-	-	29.3	15.248
9.	2MASX J00410351+4029529	Bol 199	2	-	-1.59	79.1	16.120
10.	2MASS J00425875+4108527	Bol 140	3	-413	-0.88	31.7	6.654

Notes:

¹ Following Galleti et al. (2006): 1 - confirmed globular clusters (GC), 2 - GC candidates, 3 - uncertain objects
²Total hydrogen column density based on pencil beam estimates of CO(1→0) intensity (Nieten et al. 2006), converted to molecular hydrogen column density using a constant X_{CO} conversion factor (Strong & Mattox 1996) and $\lambda 21$ cm emission from the Westerbork map (Brinks & Shane 1984).

Clouds were present during most of the observations, forcing us to use the 2MASS Point Source Catalog (Cutri et al. 1993) stars for the photometric calibration (typically using 4–10 common stars per field). No color dependence was found, and the r.m.s. of the derived zero-points was ~ 0.05 mag for both bands. The typical seeing of the optical images ($\sim 1.0''$) matches well that of the near-infrared data set ($\sim 1.5''$), allowing us to perform simple aperture photometry with $4''$ radius. We used the standard IRAF[†] tasks. The zero points of the optical data are based on stars in common with the catalog of

[†] IRAF is the Image Analysis and Reduction Facility made available to the astronomical community by the National Optical Astronomy Observatories, which are operated by AURA, Inc., under contract with the U.S. National Science Foundation.

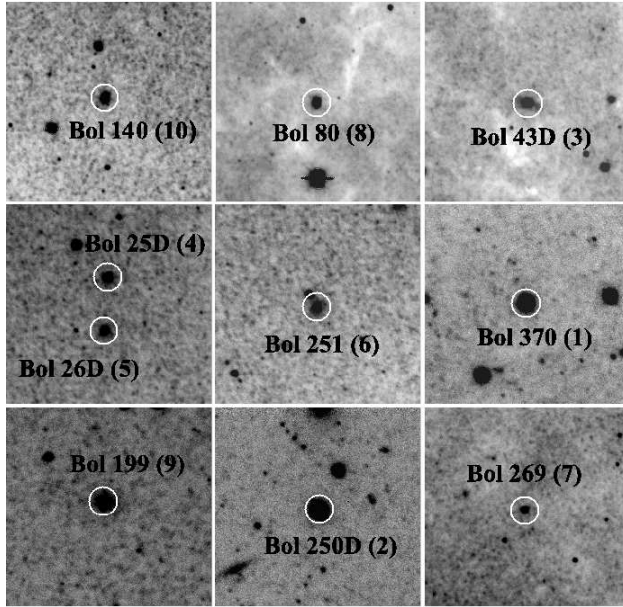


Figure 1. V -band images of our targets from the Local Group Survey (Massey et al. 2006). The field of view is $30'' \times 30''$. North is up, and East is to the left. The white circles show the photometric extraction apertures. The numbering corresponds to Table 1.

Massey et al. (2006). The V -band magnitudes and the observed colors together with their errors are listed in Table 2. The majority of the infrared colors shows excellent agreement with the available 2MASS colors (see Fig. 2).

Table 2. $UBVRHK$ photometry of the objects listed in Table 1. Photometric systems: UBV – Johnson, RI – Cousins, HK – Bessell & Brett (1988). The uncertainties include both the zero-point errors and the statistical errors of the individual measurements.

No.	V	σ_V	$U - K$	σ_{U-K}	$U - I$	σ_{U-I}	$U - R$	σ_{U-R}	$B - K$	σ_{B-K}	$V - K$	σ_{V-K}	$U - H$	σ_{U-H}
1.	16.18	0.08	3.85	0.30	2.23	0.31	1.84	0.32	3.02	0.23	2.53	0.10	3.67	0.30
2.	17.60	0.02	6.19	0.09	3.51	0.06	2.69	0.06	5.11	0.09	4.25	0.08	5.65	0.06
3.	17.15	0.02	6.46	0.05	3.90	0.06	3.08	0.05	5.16	0.07	4.21	0.05	6.13	0.06
4.	18.23	0.03	6.25	0.07	3.49	0.10	2.80	0.05	5.34	0.10	4.19	0.06	5.74	0.07
5.	18.23	0.03	5.72	0.07	3.43	0.10	2.70	0.05	4.85	0.10	3.81	0.07	5.39	0.07
6.	17.77	0.03	5.82	0.07	3.46	0.10	2.79	0.04	4.65	0.09	3.69	0.06	5.35	0.06
7.	18.49	0.03	5.83	0.09	3.51	0.07	2.96	0.06	4.68	0.11	3.72	0.09	5.31	0.09
8.	17.14	0.02	5.10	0.06	3.28	0.06	2.59	0.04	3.98	0.08	3.25	0.05	5.01	0.06
9.	18.26	0.02	6.36	0.07	3.76	0.07	2.95	0.06	5.20	0.08	4.27	0.04	5.90	0.08
10.	17.37	0.02	4.64	0.07	2.38	0.12	2.19	0.04	3.59	0.09	3.08	0.07	4.43	0.07

3. Dust properties of M31 disk from χ^2 -test minimization

The intrinsic near-infrared colors of ellipticals are nearly identical: $(H - K)_0 \sim 0.22$ mag, as demonstrated by Persson et al. (1979). Assuming all the targets belong to that Hubble

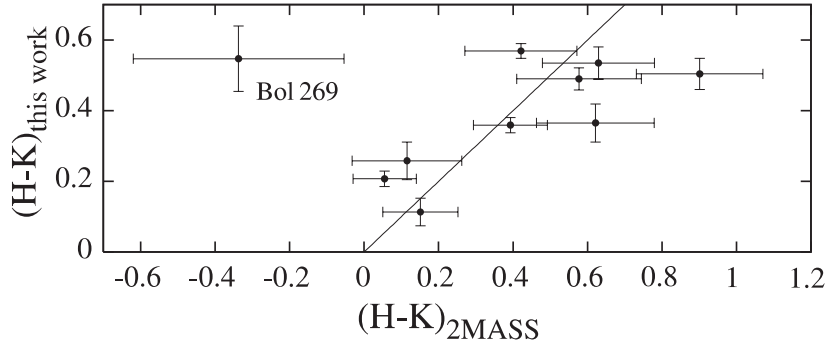


Figure 2. Comparison between the colors derived in this work and the available 2MASS colors. Note that the photometry of Bol 269 (target No.7 in our list) was flagged as suspect in the 2MASS Point Source Catalog.

type, the opacity of the disk that lay between them and the observer can easily be calculated, taking into account the internal Milky Way extinction, i.e. from the work of Schlegel et. al (1998). However, the evident contamination of the sample by globular clusters requires also to consider for each object the possibility that it is a M 31 globular, with the typical globular cluster colors. Furthermore, a cluster may be located in front of the M31 disk, adding extra degree of complication to the analysis.

To address these issues we developed a multicolor χ^2 minimization technique to derive simultaneously the disk opacity and number of other parameters: gas-to-dust ratio, extinction law and last but not least – the nature of the object (elliptical galaxy or globular cluster). It allows also to fix some of these parameters, while still varying the rest of them. The intrinsic colors of globulars were adopted from the model of Kurth et al. (1999) and for the ellipticals – from Bicker et al. (2004).

The results from the test are presented in Table 3. The free parameters in the case of globular clusters (left side of the Table 3) are: age, abundance Z , R_V , and in the case of the elliptical galaxy models (right side of the Table 3) they are: redshift z , R_V , and A_V . We created a multi-dimensional grid, with steps of 0.01 along all axes and calculated the χ^2 for every grid node.

The preliminary tests reveal that in all cases BI -bands dominate the values of χ_{min}^2 . These bands have the largest systematics with respect to external photometry (Massey et al. 2006). To account for that and to minimize their impact we tentatively added 0.20 mag to the B -band and 0.12 mag to the I -band magnitude errors. The errors listed in Table 2 do not reflect this modification. As a result, we have relatively more equal contribution of the different colors to the χ_{min}^2 .

The globular cluster model fits much better the colors of most targets than the elliptical model. The typical opacity τ_V across the M31 disk is ~ 1 mag. There are two exceptions (objects No. 8 and No. 10) for which neither model yields a reasonable match.

Interestingly, R_V in M31 is lower than the typical Galactic value of 3.1, and it is similar to the one obtained by Savcheva & Tassev (2002). This may indicate a smaller mean size of the dust grains in the diffuse component of M31 ISM, in comparison with the Milky way. Although the targets are located well within standard radius R_{25} , where the active star formation still takes place, all of them are projected in the inter-arm regions where the opacity of the disk stays relatively low, as seen from the column density values in Table 1. Here we assumed the Galactic gas-to-dust ratio (Bohlin et al., 1978).

The relation between total gas column densities and the derived extinctions, corresponding to $R_V=3.1$ and χ_{min}^2 , is plotted in Fig. 3. Surprisingly, the derived extinctions

Table 3. Summary of the χ^2 minimization. The matches of the apparent colors to the globular cluster models of Kurth et al. (1999) is given in the left and to the intrinsic colors of ellipticals predicted by the GALEV models of Bicker et al. (2004) is given on the right. The numbers of the targets as the same as in Table 1. The table also reports if the A_V corresponding to the minimum χ^2 agrees (within the errors) with the total gas density derived from the combined *HI* map of Brinks & Shane (1984) and the CO(1 \rightarrow 0) map of Nieten et al. (2006). The asterisk indicates a fixed parameter.

No.	Globular Cluster Model Fit Parameters						Elliptical Galaxy Model Fit Parameters					Derived Type
	Age [yr]	Abundance Z	R_V	A_V [mag]	χ^2_{min}	dust vs. gas?	Redshift z	R_V	A_V [mag]	χ^2_{min}	dust vs. gas?	
1.	0.9×10^9	0.0001	3.10*	1.81	1.288	no	0.000	3.10*	0.00	39.950	no	Globular
	0.9×10^9	0.0003*	3.10*	1.46	2.510	no	0.000	6.00	0.00	39.950	no	
	0.6×10^9	0.0003*	2.43	1.45	1.534	no						
2.	0.4×10^9	0.0500	3.10*	2.41	2.400	no	0.075	3.10*	0.98	7.562	yes	Globular
							0.069	3.42	1.05	6.900	yes	
3.	0.8×10^9	0.0500	3.10*	0.50	3.406	yes	0.026	3.10*	1.41	45.111	yes	Globular
	3.0×10^9	0.0009*	3.10*	2.60	19.558	no	0.021	2.15	1.18	10.404	yes	
	2.0×10^9	0.0009*	2.77	2.54	8.552	no						
4.	3.0×10^9	0.0500	3.10*	0.86	2.152	no	0.072	3.10*	1.06	7.180	no	Globular
							0.080	2.75	0.97	5.692	no	
5.	8.0×10^9	0.0400	3.10*	0.21	0.870	yes	0.046	3.10*	0.86	24.117	no	Globular
	1.1×10^{10}	0.0014*	3.10*	1.73	7.522	no	0.045	1.77	0.62	3.649	no	
	2.0×10^9	0.0014*	2.75	2.00	2.786	no						
6.	1.4×10^{10}	0.0400	3.10*	0.01	1.707	no	0.061	3.10*	0.83	69.838	no	Globular
							0.072	1.08	0.40	8.572	no	
7.	1.4×10^{10}	0.0450	3.10*	0.00	5.913	no	0.064	3.10*	0.84	61.119	yes	Globular
							0.068	1.00	0.40	13.223	yes	
8.	1.3×10^{10}	0.0200	3.10*	0.00	34.012	no	0.024	3.10*	0.56	137.883	yes	Uncertain
							0.000	1.00	0.33	27.456	yes	
9.	3.0×10^9	0.0500	3.10*	0.97	4.321	yes	0.042	3.10*	1.26	12.802	yes	Uncertain
	2.0×10^9	0.0005*	3.10*	2.67	7.154	no	0.061	2.63	1.11	9.039	yes	
	2.0×10^9	0.0005*	3.10	2.67	7.154	no						
10.	1.0×10^9	0.0500	3.10*	0.50	13.716	yes	0.042	3.10*	0.15	54.800	yes	Uncertain
	0.9×10^9	0.0025*	3.10*	2.25	26.747	no	0.000	1.00	0.15	30.674	yes	
	0.9×10^9	0.0025*	2.69	2.06	17.238	no						

of the candidate globulars (targets No. 6 and 9) correlate better with the gas density if we use intrinsic colors derived from the elliptical models. We contribute this to the spatial variations of the reddening law.

Our analysis also considers the K-correction. We used the HyperZ code of Bolzonella et al. (2000), that includes a variety of spectral energy distributions for different morphological types of galaxies. The results are presented in Table 4. Both cases – fixed to the elliptical type and free morphological types yield reasonable χ^2_{min} values. The extinction estimates are lower and the redshifts are higher than those derived earlier, indicating a degeneracy between these two quantities. The metallicity-opacity degeneracy is apparent in Table 3 as well: the higher is the abundance Z , the lower is the derived extinction and vice versa. The HyperZ tends to classify our targets as starburst galaxies, explaining the larger extinction values in comparison with the case of fixed elliptical morphological type. Note that a large fraction of the extinction may be internal to a starburst galaxy

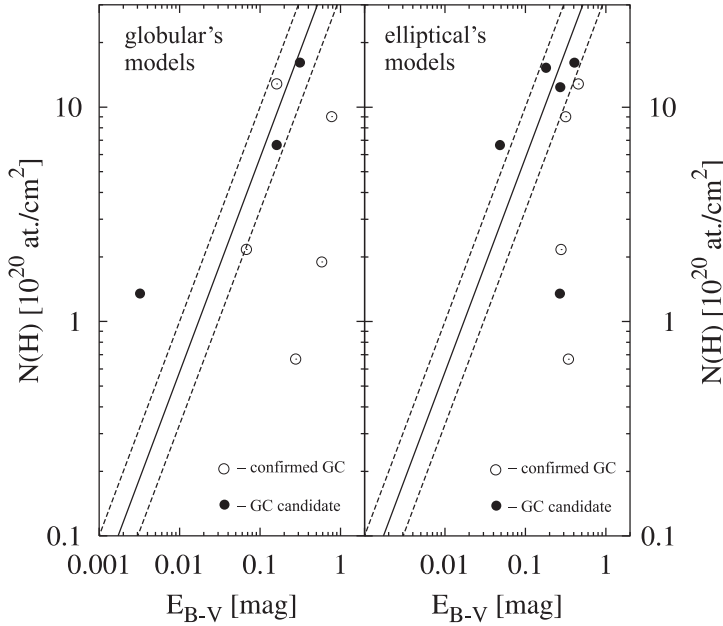


Figure 3. The agreement between the total hydrogen column density $N(H)$ and the color excess E_{B-V} with respect to Kurth et al. (1999) model colors of globulars (left) and with respect to colors of ellipticals (right) as predicted by the GALEV models (Bicker et al. 2004). The extinction values are listed in Table 2 and correspond to $R_V=3.1$ and χ_{min}^2 . Dashed lines represent the expected range and the thick line is the mean Galactic gas-to-dust ratio (Bohlin et al. 1978).

and not related to the M31 disk. This might be the case for targets No. 8 and 10 which, together with No. 9 are our best candidates for galaxies, laying behind the M31 disk.

4. Conclusions

We measure the opacity of the M31 disk from the color excesses of 21 objects – a mixture of galaxies behind the disk and globular clusters. Seven of them are consistent with globulars, two - with starburst galaxies and one - with an elliptical galaxy. Their extinction estimates are consistent with a semi-transparent disk ($\tau_V \lesssim 1$) in the inter-arm regions. We confirm the conclusion of Savcheva & Tassev (2002) that the total-to-selective extinction value R_V in the diffuse ISM of M31 is on average lower than the typical Galactic value of $R_V=3.1$. The gas-to-dust ratio appears similar to that in the Milky way and it is independent from the galactocentric distance, which might indicate Solar abundances along the line of sight studied here (within $20' \div 85'$ from the M31 center).

Acknowledgments

This work was partially supported by the following grants: VU-NZ-01/06, VU-F-201/06 & VU-F-205/06 of the Bulgarian Science Foundation. One of the authors (P.N.) thanks to organizing committee of IAU Symposium No.254 for the grant which allowed him to participate.

Table 4. Summary of the χ^2 minimization considering the K-corrections, for two different redshifts. The “intrinsic” redshifted colors of the galaxies were determined with the HyperZ (Bolzonella et al. 2000). The numbers of the targets as the same as in Table 1. The grid resolution is 0.05 along all axes and the Galactic extinction law of Allen (1976) is assumed. The rest of the columns are identical with those in Table 3.

No.	Red-shift z	A_V [mag]	χ^2_{min}	dust vs. gas?	Galaxy Type	Red-shift z	A_V [mag]	χ^2_{min}	dust vs. gas?	Galaxy Type
1.	0.130	0.05	4.562	yes	elliptical*	0.135	0.05	0.673	yes	starburst
2.	0.200	0.55	1.743	yes	elliptical*	0.200	0.55	1.743	yes	elliptical
3.	0.145	0.70	1.109	yes	elliptical*	0.140	1.00	1.025	yes	starburst
4.	0.200	0.35	1.482	no:	elliptical*	0.150	1.45	1.365	no	starburst
5.	0.150	0.25	0.546	yes	elliptical*	0.150	0.75	0.464	no	starburst
6.	0.145	0.15	2.700	yes	elliptical*	0.155	0.05	1.807	yes	starburst
7.	0.145	0.15	3.926	no	elliptical*	0.350	0.10	1.051	no	starburst
8.	0.110	0.10	2.417	no	elliptical*	0.105	0.95	2.230	yes	starburst
9.	0.155	0.75	1.246	yes	elliptical*	0.155	0.75	1.246	yes	elliptical
10.	0.050	0.00	4.659	no	elliptical*	0.150	0.50	2.571	yes	starburst

References

- Allen C. W. (1976) *Astrophysical Quantities*, (University of London: The Athlone Press), p. 264
- Battistini P., Bonoli F., Braccisi A., Fusi-Pecchi F., Malagnini M. L. & Marano B. (1980) *A&AS*, 42, 357
- Bessell M.S. & Brett J.M (2006) *PASP*, 134, 100
- Bicker J., Fritze-von Alvensleben U. & Fricke K.J. (2004) *Ap&SS*, 284, 463
- Bohlin R.C., Savage B.D. & Drake J.F. (1978) *ApJ*, 224, 132
- Bolzonella M., Miralles J.-M. & Pelló R. (2000) *A&A*, 363, 476
- Brinks E. & Shane W. (1984) *A&ASS*, 55, 179
- Cuillandre, J., Lequeux, J., Allen, R.J., Mellier, Y. & Bertin, E. (2001) *ApJ* 554, 190
- Cutri, R.M., Skrutskie, M.F. van Dyk, S. et al., *The IRSA 2MASS All-Sky Point Source Catalog, NASA/IPAC Infrared Science Archive*
- Galleti S., Federici L., Bellazzini M., Buzzoni A. & Fusi Pecci F. (2006) *A&A*, 456, 985
- Holwerda B.W., González R.A., Allen R.J. & van der Kruit P. C. (2005) *AJ*, 129, 1396
- Kurth O.M., Fritze-von Alvensleben U. & Fricke K.J. (1999) *A&ASS*, 138, 19
- Lisi F., Baffa C. & Hunt, L.K. (1993) *SPIE*, 1946, 594
- Massey P., Olsen K.A.G., Hodge P.W. et al. (2006) *ApJ*, 131, 2478
- Nedialkov P.L. & Ivanov V.D. (1998) *A&AT*, 17, 367
- Nieten Ch., Neininger, N. Guélin, M. et al. (2006) *A&A*, 453, 459
- Persson S. E., Frogel J.A. & Aaronson M. (1979) *ApJS*, 39, 61
- Savcheva A. & Tassev S. (2002) *PAOB* 73, 219
- Schlegel D.J., Finkbeiner D.P. & Davis M. (1998) *ApJ*, 500, 525
- Strong, A.W. & Mattox, J.R. (1996) *A&A*, 308, L21